MIT Open Access Articles

An analytical model for the prediction of the dynamic response of premixed flames stabilized on a heat-conducting perforated plate

An analytical model for the prediction of the dynamic response of premixed flames stabilized on a heat-conducting perforated plate

Kushal S. Kedia*, Ahmed F. Ghoniem

Reacting Gas Dynamics Laboratory,
Center for Energy and Propulsion Research,
Department of Mechanical Engineering, Massachusetts Institute of Technology.
77-Massachusetts Avenue, 3-342, Cambridge, MA, 02139, USA

Abstract

The dynamic response of a premixed flame stabilized on a heat-conducting perforated plate depends critically on their coupled thermal interaction. The objective of this paper is to develop an analytical model to capture this coupling. The model predicts the mean flame base standoff distance; the flame base area, curvature and speed; and the burner plate temperature given the operating conditions; the mean velocity, temperature and equivalence ratio of the reactants; thermal conductivity and the perforation ratio of the burner. This coupled model is combined with our flame transfer function (FTF) model to predict the dynamic response of the flame to velocity perturbations. We show that modeling the thermal coupling between the flame and the burner, while accounting for the two-dimensionality of the former, is critical to predicting the dynamic response characteristics such as the overshoot in the gain curve (resonant condition) and the phase delay. Good agreement with the numerical and experimental results is demonstrated over a range of conditions.

Keywords: flame transfer function, perforated-plate, dynamic response, flame-wall interaction, laminar

*Corresponding author: kushal@mit.edu

1. Introduction

Perforated-plate stabilized premixed flames are used extensively in industrial and compact household burners. In these systems, the coupling between the acoustics and the unsteady heat release rate often leads to self-excited oscillations, which in extreme cases may result in fatal structural damage. The dynamic response of the flame to velocity perturbations determines the nature of the combustion instability. This response is typically characterized by the flame transfer function (FTF). A linear FTF is defined as $\text{TF}(f) = \frac{Q'_f/Q_f}{U'/U}$, where f is the frequency of the velocity perturbations (U') and Q_f is the net heat release rate.

Durox et al. [1] experimentally investigated the dynamic flame response under different configurations and determined that at certain low frequencies, the normalized heat release amplitude is greater than the non-dimensional velocity oscillations. For V-shaped and M-shaped flames, resonance (overshoot in the FTF gain) was attributed to flame-area oscillations. Such experimental investigations of FTF were first performed by Sugimoto and Matsui in [2] to analyze the so-called 'pyro-acoustic amplification'. In recent investigations, it was shown that for perforated-plate burners, this behavior arises because of a significant thermal interaction between the gases and the plate [3, 4, 5]. We also recently elucidated the mechanism of the stabilization of flames on perforated-plate burners highlighting the coupled role of curvature and local heat loss to the burner top using numerical simulations with detailed chemistry [6]. The flame anchors at a finite standoff distance away from the plate, thereby fixing the plate temperature depending on the thermal boundary conditions [6, 7]. The standoff distance undergoes finite oscillations during an unsteady cycle [5], resulting in flame base speed perturbations. These must be accurately estimated for any experimental, numerical or analytical investigation of FTF.

FTFs were experimentally investigated for perforated-plate burners in [3] (rectangular-slits) and in [8] (circular-holes). A systematic parametric investigation was carried out on externally cooled plates. However, the temperature

of the plate surface was not accurately measured and was reported to be 100-150 C. Boudy et al. experimentally obtained nonlinear flame response (flame describing functions FDF) for flames stabilized on perforated plates in [9] and performed thermoacoustic analyses.

An analytical model for the prediction of perforated-plate stabilized FTFs was proposed by Altay et al. [4]. The model incorporated the effects of the two-dimensionality of the flame, its area fluctuations and the heat exchange with the plate. However, it relied on specifying the steady-state flame standoff distance which was obtained from the perforated-plate's surface temperature using Rook's model [10, 11]. This plate temperature was a free parameter in the model in [4]. The model further assumed that the mean burning velocity of the flame base is the adiabatic laminar flame speed. These assumptions encompass the flame-wall thermal interaction information, which we demonstrated to be critical in determining the FTFs using detailed chemistry numerical simulations in [5]. In these 2D dynamic simulations, we showed that the heat exchange rate oscillations plays an important role in driving the growth of the perturbations over a wide range of conditions, including resonance. Similar 2D simulations were performed in [12]. They fixed the burner wall temperature at 373 K and 430 K for rectangular-slit and round-holed perforated plate respectively, because the fluid and the solid domains were not coupled in their numerical model. However, the plate surface and the duct wall temperatures are not free parameters in a practical burner.

In this paper, we improve the analytical model described in [4]. We describe a model that predicts the perforated-plate surface temperature and flame stand-off distance, among other relevant quantities, given the operating conditions. We show the model's validity using our numerical simulations from [5, 6] and compare with the experimental results of Manohar [8].

3

2. Governing Equations

Figure 1a schematically illustrates a two-dimensional slice of an axis-symmetric bell-shaped premixed flame stabilized on a heat conducting plate. Figure 1b shows a top-view of the perforated-plate burner. A co-ordinate system $r - x$ is used. The control volume under consideration is shaded in Fig. 1a. It includes the solid burner region, additionally marked by hashed lines. The part of the flame above the burner plate and within the shaded region in Fig. 1a is referred to here as the flame base. In this section, we develop the governing equations to predict the steady-state physical quantities given the mean inlet velocity, U, through inner hole of perforated-plate; equivalence ratio ϕ; thermal conductivity of the plate (or flame-holder) λ_{fh} and the perforation ratio $\kappa = R_o/R_i$. R_o is the outer radius of the domain and R_i is the inner hole radius. U is assumed to be constant across $0 < r < R_i$. T_u, ρ_u are the temperature and the density of the unburnt reactants.

δ_T is the flame base standoff distance. We assume that the temperature at the flame base (where the reaction rate is zero) is the burnt gas temperature, T_b. This assumption over-estimates the flame base temperature. The actual value at that location is lower due to factors such as incomplete oxidation of CO and heat losses to the surroundings. There is typically a small recirculation zone region within δ_T that plays an important role in the overall stability of the flame [6]. δ_R is the reaction zone thickness where the reaction rate is finite and high, which lies immediately above the recirculation zone. For modeling simplicity, we assume that δ_T and δ_R are the mean characteristic distances of the entire flame base. This is an approximation because the flame base is often highly curved, with its curved area, A_F, greater than the flame holder area, $A_{fh} = \pi(R_o^2 - R_i^2)$. The thickness of the plate is denoted by L. The specific heat, $c_{p,u}$, and the thermal conductivity, λ_u, of the mixture are assumed constant throughout the domain at their unburnt values.

The outer (due to periodicity) and the inner streamwise edges of the shaded domain in Fig. 1a are modeled as adiabatic slip walls. This is chosen to separate

the flame base region from the flame tip region, such that $A_i^*/\pi R_i^2 = A_{fh}/\pi R_o^2$. A_i^* is the cross-sectional area of the shaded region of the inner hole (see Fig. 1b). This relation suggests that at each streamwise location of the control volume, the fraction of the total cross-sectional area occupied by the streamtube under consideration is the same. The flame base speed is denoted by S_F. Mass conservation in the shaded control volume is

$$\rho_u U A_i^* = \rho_u S_F A_F \tag{1}$$

We assume that the density at the unburnt side of the reaction front (where the flame speed S_F is to be estimated) is ρ_u for simplicity. The actual value is slightly lower due to the preheating via heat recuperation from the burner, as discussed later. Similar to δ_T and δ_R, S_F is also an average over the curved flame base. The energy conservation, assuming an overall adiabatic system, is

$$\rho_u U A_i^* c_{p,u}(T_b - T_u) = \bar{w}_f \Delta H_{R,f} \delta_R A_F \tag{2}$$

where $\bar{w}_f$ is the average volumetric fuel consumption rate and $\Delta H_{R,f}$ is the heat of reaction of the fuel (methane). The adiabatic assumption is consistent with our previous numerical work in [6, 7]. However, the burner plate may be externally cooled as discussed in [3, 8]. Including this non-adiabaticity is a natural extension of our model; however the focus of this paper is to see the critical impact of the internal parameters of the system alone on the physical quantities of interest. $\bar{w}_f \Delta H_{R,f}$ is estimated using our one-dimensional simulations in [7]. The consumption speed of a flame, S_c, defined on the basis of the rate of energy consumption, is used because it does not depend significantly on the flame curvature [6, 13]. For a given ϕ and T_u; the 1D flame thickness δ_R^o, T_b and the adiabatic laminar flame speed S_L^o (equal to its consumption speed for one-dimensional adiabatic unstretched flames),

$$\bar{w}_f \Delta H_{R,f} = \frac{\rho_u S_L^o c_{p,u}(T_b - T_u)}{\delta_R^o} \tag{3}$$

We assume that the temperature increases linearly from $T_{fh,0}$ to T_b in the region above the flame-holder, where $T_{fh,0}$ is the plate surface temperature. Hence the

5

average heat flux on the top of the flame-holder

$$\dot{q}''_{fh} = \frac{\lambda_u (T_b - T_{fh,0})}{\delta_T} \tag{4}$$

The heat transfer to the burner plate's top surface re-enters into the reactants from the inner-hole wall. The balance of this recirculated heat is

$$\dot{q}''_{fh} A_{fh} = \rho_u U A_i^* c_{p,u} (T_{i,0} - T_u) \tag{5}$$

where $T_{i,0}$ is the mean temperature of the reactants exiting the inner hole. The flame base geometry is assumed to be parabolic with its axis as the periodic outer edge of the domain and curvature $\gamma = \frac{d^2 x_F}{dr'^2}$ at the tip of the parabola (where $r' = R_o - r$). The area of the flame base is larger than A_{fh} for positively curved (concave towards products side) flame base. We assume a circular burner surface area for simplicity. The flame base above the burner plate can then be represented as $\frac{dx_F}{dr'} = -\gamma r'$ and its base area is approximately

$$A_F = \int_{R_i}^{R_o} 2\pi (R_o - r) \sqrt{1 + \gamma^2 (R_o - r)^2} dr \tag{6}$$

Due to double-periodicity, the perforations and the flames form an artificial ring-like pattern. The integration in Eq. 6 to estimate the curved flame area, can also be performed along a circle with an origin at inner axis rather than at the outer periodic edge. We found that the results do not change with this modification. High activation energy asymptotics [14] is used to approximate the relative size of the reaction zone thickness to the flame standoff distance, which is equivalent to a thermal thickness of the flame base. For chemical reaction with overall reaction order n, Zeldovich number $Z = \frac{T_a}{T_b^2}(T_b - T_u)$ (T_a is the activation temperature of the fuel) and the ignition temperature T_{ig},

$$\frac{T_b - T_{ig}}{T_b - T_u} = \frac{n}{Z} \tag{7}$$

Ignition corresponds to the start of the reaction zone. Hence geometrical constraint results in

$$\frac{T_b - T_{ig}}{T_b - T_{fh,0}} = \frac{\delta_R}{\delta_T} \tag{8}$$

6

The governing equations that determine the thermal coupling between the plate and the fluid depend on the burner geometry and the natural thermal boundary conditions. There is a temperature gradient within the plate if the Biot number, based on the plate thickness, $h_c L/\lambda_{fh} > 0.2$, where h_c is a convective heat transfer coefficient. The resulting temperature profile within the burner plate and the bulk temperature of the fluid in the inner hole is denoted by $T_{fh,x}$ and $T_{i,x}$ respectively. The subscripts fh and i denotes the flame-holder (burner plate) and the inner hole respectively; and x denotes their variation in that direction. The corresponding burner surface temperature and the exit hole temperature are given by $T_{fh,0}$ and $T_{i,0}$, discussed in Case A. Alternatively a thin plate, with a small Biot number (illustrated in Fig. 1c) used in the experiments in [3, 8], can be modeled as being isothermal as discussed in Case B. In both the cases, the Biot number based on the characteristic radial dimension, $h_c(R_o - R_i)/\lambda_u < 0.2$, for the typical burner geometries used in this paper and hence we neglect any radial variation in T_i and T_{fh}.

Case A: Fin approximation for a thick plate

There is a laminar flow through the inner hole of the perforated plate. An average Nusselt number for the convective heat transfer ≈ 4 [15], resulting in $h_c = \frac{2\lambda_u}{R_i}$. Similar to fin analysis [15], the governing equation within the flame-holder is

$$\lambda_{fh}\frac{d^2 T_{fh}(x)}{dx^2} = 2\pi R_i h_c (T_{fh}(x) - T_i(x)) \tag{9}$$

with the boundary conditions as $T_{fh}(x = 0) = T_{fh,0}$ and $\frac{dT_{fh}(x)}{dx}(x = L) = 0$. Similarly, the governing equation for the bulk motion of the fluid within the hole is

$$\rho_u U A_i^* c_{p,u} \frac{dT_i(x)}{dx} = -2\pi R_i h_c (T_{fh}(x) - T_i(x)) \tag{10}$$

with the boundary condition at the inlet of the hole as $T_i(x = L) = T_u$. The ordinary differential Eqs. 9 and 10 are simultaneously solved numerically to obtain $T_{fh}(x)$ and $T_i(x)$. Using the solution, we obtain the exit hole bulk

temperature of the fluid

$$T_{i,0} = T_i(x = 0) \tag{11}$$

Case B: Isothermal thin plate

In this case, the natural boundary condition corresponds to the heat being convected upstream from the thin perforated plate, illustrated in Fig. 1c. The average convective heat transfer coefficient, h_{pp} can be estimated using the Nusselt number correlation for convective heat transfer from an isothermal perforated plate to upstream impinging reactants [16],

$$h_{pp} = 0.881 \frac{\lambda_u}{L*} (\frac{2R_i U}{\nu_u})^{0.476} \mathrm{Pr}^{\frac{1}{3}} \tag{12}$$

where $L* = A_{fh}/(2R_o)$. We take $\mathrm{Pr} = 0.69$ and $\nu_u = 1.5 \times 10^{-6} \mathrm{m}^2/\mathrm{s}$. The heat transferred upstream from the isothermal perforated-plate increases the sensible enthalpy of the incoming reactants such that

$$\rho_u U A_i^* c_{p,u}(T_{i,0} - T_u) = h_{pp} A_{fh}(T_{fh,0} - T_u) \tag{13}$$

In both the cases, it is assumed that the heat lost to the environment is negligible. This may not be the case for externally cooled plate, as in the experiments in [3, 8].

2.2. Hypothesis

In the governing equations, S_F is an average flame base speed. The local flame structure above the flame holder, at the curved base, was discussed in detail in our recent numerical investigation [6]. We showed that the unburnt side of the reaction front is immediately above the stagnation point of the recirculation zone over the burner plate. Hence, we assume here that the edge of the parabolic flame base has a zero local flame displacement speed. The structure of the flame wing resembles that of a one-dimensional flame as the influence of the burner wall is reduced. Thus we assume a linear decrease of the flame speed from S_L^o at the inner edge to zero at the outer periodic edge of the shaded region

in Fig. 1a. The area averaged flame speed is then

$$S_F = \frac{1}{A_F} \int\limits_{R_i}^{R_o} \frac{S_L^o(R_o - r)}{R_o - R_i} 2\pi r \sqrt{1 + \gamma^2(R_o - r)^2} dr \qquad (14)$$

Depending on the boundary conditions, Eqs. 1-11 and 14 or Eqs. 1-8 and 12-14 form a complete set of nonlinear equations. These are solved simultaneously to obtain the physical quantities of interest δ_T, δ_R, $T_{fh,0}$, $T_{i,0}$, γ, S_F, A_F and $\dot{q}''_{fh}$, given the operating parameters ϕ, U, κ, λ_{fh}, T_u.

2.3. FTF model

Altay et al. [4] developed an analytical model to predict FTFs by assuming a series of plane and conical flame fronts above the perforated-plate to account for two-dimensionality. The kinematics of 2D flame surfaces were modeled, extending the assumptions of Fleifil et al.[17] to couple the flame surface kinematics equation with the heat loss to the burner plate. In this paper, we improve on this model, however only the major changes are highlighted[1].

The flame speed above the burner plate ($\bar{S}_u$ in [4]), which was assumed to be S_L^o, is modified to S_F. The burnt gas temperature ($\bar{T}_b$ in [4]) was assumed to be a free parameter to account for non-adiabaticity. This is changed to the adiabatic value since we have developed an overall adiabatic model. $T_{fh,0}$ was accounted for in the form of the density weighted flame stand off distance, $\bar{\psi}_{fp}$, which was estimated using Rook's logarithmic model in [11]. This is replaced here by the average temperature weighted flame standoff distance, $\frac{\bar{\psi}_{fp}}{\delta} = 1.5 \frac{\delta_T}{\delta} \frac{T_u}{T_b}$. $\delta = \frac{\lambda_u}{rho_u c_{p,u} S_L^0}$ is a reference thermal thickness of the flame. The factor of 1.5 is used because it provided a reasonable agreement with the FTFs from our numerical simulations, discussed in Sec. 3.

3. Results and Discussions

The discussions in this section are divided into three parts. First, the steady-state model described in this paper is validated using our numerical simulations

---

[1]Nomenclature in [4]: $T_s = T_{fh,0}$, $A_{open} = \pi R_i^2$, $A_u = \pi R_o^2$ and $A_p = A_{fh}$

from [7, 6]. The results of the steady-state model coupled with the FTF model described in Section 2.3 are then compared to the numerical simulations in [5] at the same operating conditions. Lastly, we compare our model results to the experimentally obtained FTFs from [8]. The parameters that are kept constant throughout the analysis are, $R_i = 0.5$ mm; the plate thickness, $L = 13.2$ mm (except in Section 3.3 where the plate is very thin), $T_u = 300$ K, $\rho_u = 1.15$ kg/m^3, $c_{p,u} = 1059.4$ J/kgK, $\lambda_u = 0.0275$ W/mK, lower heating value of methane $LHV = 50.1$ MJ/kg, $T_a = 24400$ K and order of reaction $n = 1.9$. S_L^o, δ_R^o and T_b depend on ϕ and T_u and the values are determined using our 1D simulations in [7]

3.1. Steady-state Model Validation and Verification

Fig. 2 shows good agreements for $T_{i,x}$ and $T_{fh,x}$ obtained using the model and simulations at different operating conditions. The natural boundary conditions discussed in Sec. 2.1 Case A are used in the model. The temperature field from the simulations was averaged in the radial direction to obtain a variation with x. The plate temperature increases as ϕ and κ grow. Moreover, the standoff distance predicted by the model is of the same order of magnitude as seen in the simulations. The standoff distance depends on the definition of the flame front. For example, for the case with $U = 1.3$ m/s, $\phi = 0.75$ and $\kappa = R_o/R_i = 2$, the model predicts $\delta_T = 1.49$ mm and $\delta_R = 0.29$ mm. This is in close agreement with the values obtained from the simulations for $T = 0.9 \times T_b$ contour [6]; $\delta_T = 1.3$ mm and $\delta_R = 0.4$ mm, computed at the periodic edge of the domain where there flame is the closest to the burner plate.

We numerically demonstrated the increase in the flame standoff distance, and decrease in the burner temperature as U grows in [6]. In [7] we showed that δ_T decreases and $T_{fh,0}$ increases as ϕ or κ were increased at a constant U. Figure 3 shows that all these trends are well captured in the model with the changing operating (ϕ, κ, U). It also shows a good agreement in $T_{fh,0}$ between the model and the simulation results for $\phi = 0.75$ and $\kappa = 2$ for a wide range of U.

3.2. FTF comparison with numerical simulations

In this section, we discuss the impact of the operating conditions on the FTFs obtained using the model and compare them with the simulations in [5]. Figures 4 and 5 show the gain and the phase of the response at different operating conditions.

The overall shape of the FTF of such heat conducting perforated-plate burner are discussed in detail in [3, 4, 5]. The model predicts rather well the FTFs in all the conditions of interest. At low frequencies, as the flame moves away / towards the burner, its burning velocity increases / decreases, amplifying the flame motion at certain frequencies, the gain overshoots unity and exhibits a resonance behavior. The flame responds weakly to high frequency oscillations (diminishing gain in FTF), due to quick dissipation of small scale-structures in the flame. There is a time delay associated with the convection time needed for the reactants to reach the flame base, $\tau \sim \delta_T/S_F$ [5]. Depending on the frequency of the imposed velocity oscillations, f, the convective time delay results in a phase difference of $2\pi\tau f$, growing linearly with frequency as we observe in Fig. 4 and 5. The resonant frequency is likely to depend on this time lag, $f_{res} \sim 1/\tau \sim S_F/\delta_T$. For $U = 1.3$ m/s, $\phi = 0.75$ and $\kappa = 2$, our model predicts $S_F/\delta_T \approx 80$ Hz, which is very close to the f_{res} seen in Fig. 4. S_F/δ_T predicts f_{res} reasonably well for all the other cases also. Similar dependency is noted in [4, 8]. We demonstrated in [5] that the flame-wall interaction is a critical mechanism which results in the observed resonance, which is completely missed if a perfectly adiabatic burner plate is assumed. The slope of the phase curve changes near the resonant frequency, showing that the large amplitude oscillations near the resonant condition alters the time lag, also observed by Durox et al. [1]. The physical mechanism of the system's affinity to certain low frequencies for an under-damped response is still unclear.

Figures 4 and 5 show that the low frequency response of the FTF (both in gain and phase) is captured reasonably well by the model. The resonance frequency shifts to the right and the phase delay decreases as the plate temperature increases or the standoff distance decreases, as seen when U changes

from 1.3 m/s to 0.8 m/s in Fig. 4, and when ϕ increases from 0.75 to 0.85 in Fig. 5. This is also consistent with the hypothesis that $f_{res} \sim 1/\tau \sim S_F/\delta_T$. Similar trends are observed when κ increases from 2 to 3. Thus, the plate temperature and the standoff distance must be accurately predicted to capture the correct dynamics. In the experimental results in [8], the resonant frequency increases with U contrary to the results shown here, because of the additional influence of the external cooling on δ_T when U (or equivalently S_F) changes. Since $f_{res} \sim S_F/\delta_T$, the shift in resonant frequency will depend on this modified thermal boundary condition.

It was shown in [4] that at low frequencies with respect to f_{res}, the contribution of flame area oscillations to the net heat release rate is weak compared to that of the burner heat loss oscillations, resulting in the rapid increase in the phase lag. For $f > f_{res}$, only flame area oscillations contribute to the net heat release rate fluctuations, which arise as a result of the inlet velocity fluctuations, saturating the phase behavior. The model predictions are poor compared to the simulations near the frequency where the phase saturates; this is the cut-off frequency of our model f^*. In all the FTF phase curves obtained using our model, we see that $f^* \approx 1.5 \times f_{res} \sim 1.5 \times S_F/\delta_T$. $f^* \approx 140$ Hz for the cases shown in Fig. 4. We note that f^* is a result of the assumptions of our analytical model and is not a physical quantity.

Several factors account for the quantitative differences between the predictions in Figs. 4 and 5 using the model and in simulations. The dynamic response model used from [4] does not account for increased flame base area due to curvature. We also assumed complete adiabaticity, whereas there may be some heat loss to the inner streamtube which was thermally detached in our assumptions. Lastly, the application of Rook's model to the plane front of the flame over the burner in [4] to predict its burning velocity oscillations is incorrect in strictest sense because it was mainly developed for one-dimensional flat flames over non-adiabatic porous burners.

Impact of thermal conductivity

Figure 6 shows the impact of the plate thermal conductivity on its surface temperature; the gain and phase of the FTFs. The impact quickly saturates as we move away from a ceramic and other low conductivity material. The 'resonance' behavior of such burners can thus be controlled if the burner plate is made of low thermal conductivity material. The dependency of the system dynamics on λ_{fh}, including the saturation for high λ_{fh}, was also shown by McIntosh and Clarke in [18] for flat flames stabilized over cooled porous-plug type of flame-holders, where they reviewed models determining the flame stand-off distance and its temperature. The thermal conductivity plays a role in determining $T_{fh,0}$ through Eqs. 9 and 11 developed for thick plates. This is not the case for isothermal thin plates as can be seen through Eqs. 12-13.

3.3. FTF comparison with experiments

In this section we show that our model qualitatively predicts the FTFs in [8]. We use an isothermal plate, which is the natural boundary condition for thin plates (discussed in Sec. 2.1, Case B), since the Biot numbers, $h_c L/\lambda_{fh} < 0.2$ and $h_c(R_o - R_i)/\lambda_{fh} < 0.2$ for thin plates (see schematic illustration in Fig. 1c). Figure 7 shows a comparison between the predicted FTF assuming overall adiabaticity and the experimental FTFs in [8] determined in the presence of external cooling of the plate. We qualitatively capture the trends of the experiment showing that the non-adiabaticity must be introduced in the model. Moreover, the amount of external cooling in [8] is likely to depend on ϕ, because at high ϕ the flame is closer to the plate, increasing the plate temperature, which will likely increase its non-adiabaticity.

The FTFs depends on the accurate estimation of $T_{fh,0}$ and δ_T. These quantities are coupled and their relationship will be strongly influenced when there is an additional external control over the thermal boundary conditions of the system, such as external cooling of the burner plate. This is a major reason that some trends of the FTFs in [8] were reported to be different from those predicted in [5]. The secondary peak, seen at high frequencies (around 500 Hz)

in the experimental results in [8], are not reproduced in our FTF model. This secondary peak is also missing in our numerical simulations [5], although a finite gain at high frequencies is predicted due to the detailed length scale resolution of the flame structure. This is currently under investigation.

4. Conclusions

A coupled analytical model for perforated-plate stabilized flames has been developed to predict the burner surface temperature, flame standoff distance, flame base speed, area and curvature given the operating conditions. We validated the model using our detailed numerical simulations data from [6, 7]. The mean flame standoff distance and the flame base speed are used as inputs to the linear flame transfer function model described in [4]. The two models are coupled and used to predict the linearized dynamic response of the flame to velocity perturbations. Under-damped oscillations resulting in gain overshooting unity (resonance) and the phase lag behavior are recovered. The resonant frequency, $f_{res} \sim S_F/\delta_T$, depends on the thermal coupling between the flame and the heat loss to the burner surface. This coupling manifests itself in the burner surface temperature and the flame stand-off distance. Thus models used to predict such flame dynamics must capture their dependency. Our FTF model resolves only the large length-scales of the system; as a result high frequency response, beyond the model cut-off frequency f^*, is not accurately predicted. For $f < f^*$, the FTFs are in good agreement with the numerical simulations in [5], with all the trends predicted correctly. By changing the thermal boundary conditions to match the experiments in [8], good qualitative predictions are also achieved showing that non-adiabaticity, to account for heat losses to the environment, needs to be incorporated in the model. The flames are modeled as a series of conical flame front over the holes and plane flame fronts above the burner in the FTF model in [4]. The dynamic response of the plane flame-front was predicted using the Rook's model developed for 1D flat flames above a porous burner in [10]. This mismatch is a limitation in our FTF model, which needs

14

to be addressed. These modifications to the model are currently underway. A mechanistic understanding of the resonance behavior is still unclear and is also under investigation using our fluid-solid coupled numerical simulations.

5. Acknowledgments

References

[1] D. Durox, T. Schuller, N. Noiray, S. Candel, *Proc. Combust. Inst.* 32 (2009) 1391–1398.

[2] T. Sugimoto, Y. Matsui, *Nineteenth Symposium (International) on Combustion* 19 (1) (1982) 245 – 250.

[3] V. Kornilov, R. Rook, J. ten Thije Boonkkamp, L. de Goey, *Combustion and Flame* 156 (2009) 1957–1970.

[4] H. M. Altay, S. Park, D. Wu, D. Wee, A. M. Annaswamy, A. F. Ghoniem, *Proc. Combust. Inst.* 32 (2009) 1359–1366.

[5] K. S. Kedia, H. M. Altay, A. F. Ghoniem, *Proceedings of the Combustion Institute* 33 (2011) 1113–1120.

[6] K. S. Kedia, A. F. Ghoniem, *Combustion and Flame* 159 (2012) 1055–1069.

[7] H. M. Altay, K. S. Kedia, R. L. Speth, A. F. Ghoniem, *Combustion Theory and Modelling* 14 (2010) 135–154.

[8] M. Manohar, *Thermo-Acoustics of Bunsen type premixed flames*, Ph.D. thesis, Eindhoven University of Technology, Eindhoven, The Netherlands (2011).

[9] F. Boudy, D. Durox, T. Schuller, S. Candel, *Proceedings of the Combustion Institute* 33 (2011) 1121–1128.

[10] R. Rook, L. P. H. de Goey, L. M. T. Somers, K. R. A. M. Schreel, R. Parchen, *Combustion Theory and Modeling* 6 (2002) 223–242.

[11] R. Rook, *Acoustics in Burner Stabilized Flames*, Ph.D. thesis, Eindhoven University of Technology, Eindhoven, The Netherlands, http://www.tue.nl/bib/ (2001).

[12] F. Duchaine, F. Boudy, D. Durox, T. Poinsot, *Combustion and Flame* 158 (2011) 2384–2394.

[13] T. Poinsot, T. Echekki, M. G. Mungal, *Combustion Science and Technology* 81 (1992) 45–73.

[14] I. Glassman, R. A. Yetter, *Combustion*, Academic Press New York, 2008.

[15] A. F. Mills, *Heat Transfer*, Prentice Hall, Inc., 1999.

[16] E. M. Sparrow, M. C. Ortiz, *International Journal of Heat and Mass Transfer* 25 (1982) 127–135.

[17] M. Fleifil, A. M. Annaswamy, Z. A. Ghoneim, A. F. Ghoniem, *Combustion and Flame* 106 (4) (1996) 487–510.

[18] A. C. McIntosh, J. F. Clarke, *Combustion Science and Technology* 37 (3-4) (1984) 201–219.
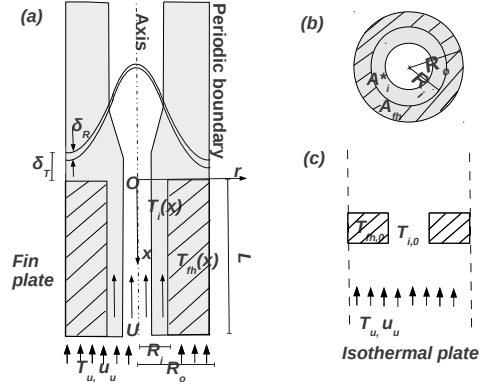
List of Figures

17

Figure 1: (a) Schematic illustration of the analytical domain with a thick flame holder to use fin approximation ; (b) Top view of the burner shown in part (a) ; (c) Isothermal plate illustration to model a thin flame holder, to compare the flame transfer function model with the experimental results in [8]
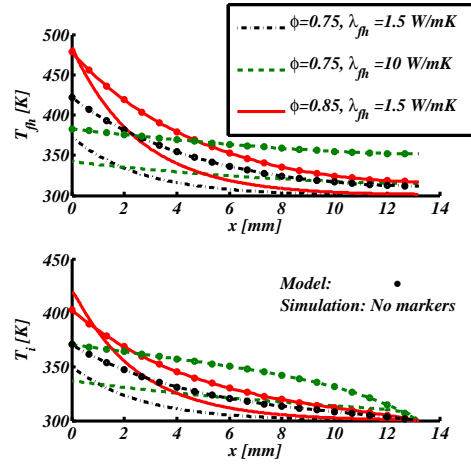
.

Figure 2: Mean temperature profiles, $T_{fh}(x)$ and $T_i(x)$, validation of the model using our two-dimensional steady-state simulations described in [7] for the case: $\kappa = 1$, $U = 1.3$ m/s
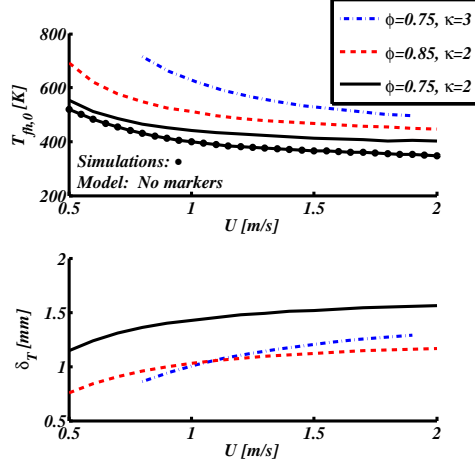
Figure 3: Plate temperature and the flame standoff distance predicted using the model for burner with $\lambda_{fh} = 1.5$ W/mK as function of the mean inlet velocity at different equivalence ratio and perforation ratio. The average plate temperature computed from simulations in [5] is also shown for the case with $\phi = 0.75$, $\lambda_{fh} = 1.5$ W/mK and $\kappa = 2$
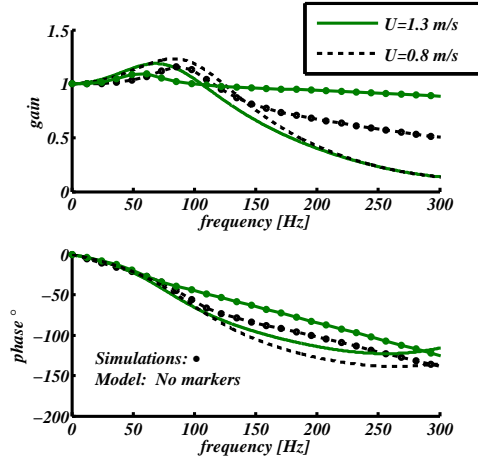

Figure 4: FTF comparison with simulations in [5] for the cases with $\phi = 0.75$, $\kappa = 2$ and $\lambda_{fh} = 1.5$ W/mK
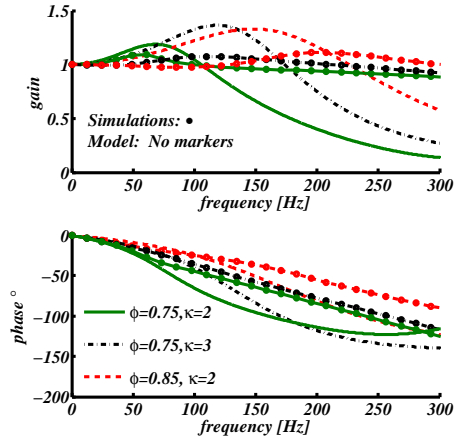
19

Figure 5: FTF comparison with simulations in [5] for the cases with $U = 1.3$ m/s, $\lambda_{fh} = 1.5$ W/mK

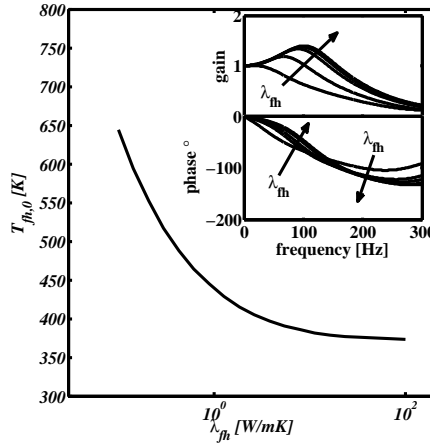Figure 6: Variation of the plate temperature predicted using the model for fixed $\phi = 0.75$, $\kappa = 2$ and $U = 1.3$ m/s at different thermal conductivities of the burner. The inserted figure shows gain and phase of FTF as λ_{fh} is increased
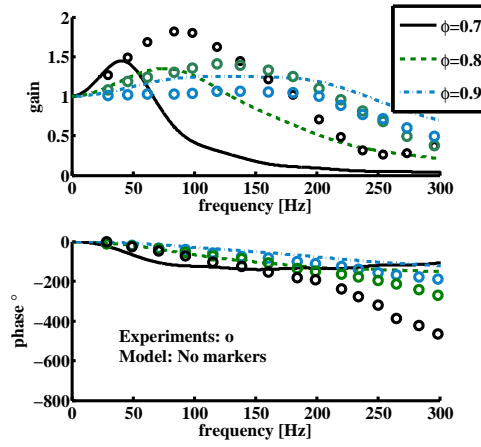
20

Figure 7: FTF comparison with experiments in [8] at different equivalence ratios for the cases with $U = 1.25$ m/s and $\kappa = 1.5$.